Exploring energy transfer in a metal/perovskite nanocrystal antenna to drive photocatalysis

Seryio Saris, [a] *Anna Loiudice,*[a] *Mounir Mensi,*[b] *Raffaella Buonsanti**[a]

[a] Laboratory of Nanochemistry for Energy (LNCE), Institute of Chemical Sciences and Engineering (ISIC), École Polytechnique Fédérale de Lausanne, CH-1950, Sion, Switzerland.

[b] Institute of Chemical Science and Engineering (ISIC), École Polytechnique Fédérale de Lausanne, CH-1950 Sion, Switzerland.

KEYWORDS: perovskites, nanocrystals, energy transfer, photochemistry

ABSTRACT: The use of all-inorganic perovskite nanocrystals (PeNCs) in photocatalytic systems has been limited due to their instability in polar solvents. Encapsulation of PeNCs in inorganic and polymeric matrices has been shown to be effective in overcoming such instability issues, yet studies on charge/energy extraction from these composite systems are still rare. Herein, we explore the capacity of CsPbBr3 PeNC/AlOx composite films to drive chemical reactions by coupling them to plasmonic AgNCs. AlOx is used both as a stabilizing layer and as a spacer to study

distance-dependent excitation energy transfer, which reveal a unidirectional migration of energy from the PeNCs towards the AgNCs. We then utilize this pooled energy for a plasmon-mediated methylene blue desorption where we demonstrate enhancement effects of spectral and spatial absorption on the reaction outcome due to the coupling to PeNCs.

Spatial migration of electronic energy plays a crucial role within the natural photosynthetic system. Solar energy is captured by multiple light-absorbing antenna complexes and funneled into a single catalytic centre via Förster resonance energy transfer (FRET), hence providing spectral and spatial amplification of absorption at the relatively low-flux conditions of solar irradiation (10^{15} ph cm^{-2} s^{-1}).[1,2] In the past decades, a variety of artificial systems inspired by the photosynthetic concept of absorption amplification have been studied, including molecular photocatalysts, inorganic biological hybrids, and fully inorganic metal/semiconductor assemblies.[3–12] However, most of these studies are based on charge transfer rather than energy transfer processes, where upon light absorption by the sensitizer, the catalyst acts as an electron/hole sink, separating charges and driving the relevant chemical reaction. FRET mediated sensitizing schemes are rare, yet these weakly coupled energy migration systems can be used to avoid exciton-exciton annihilation within the absorbers and provide a more energy-conserving alternative to charge transfer systems in polar environments.[4,13,14]

Throughout the literature on artificial photosystems, conventional II-VI semiconductor nanocrystals (NCs) are among the most utilized sensitizers due to their wide spectral absorption, easy tunability of their optical and electronic properties, and versatile surface chemistry.[15,16] Neverthless, the sensitivity to surface defects of these NCs contributes to photoluminescence quenching and limits the energy transfer efficiencies, thus reducing the overall function of the

sensitizer in the hybrid architectures.[16] Conversely, the more recently discovered all-inorganic perovskite NCs ($CsPbX_3$, X= Cl, Br, I) possess exceptionally high photoluminescence and quantum yields (>80%) and a highly defect-tolerant electronic structure.[17–19] Therefore, they have been extensively used for light-emitting and lasing applications,[20–26] but reports on their light-harvesting properties as part of an artificial photosystem are still scarce.[27–29] Structural and optical instability issues caused by light and polar solvents are the main challenges in employing perovskite NCs in complex photocatalytic architectures.[19] It is unknown whether stabilization methods that are useful for light-emitting applications, such as encapsulation in organic and inorganic matrices,[30–33] can be applied to light-harvesting applications due to the anticipated difficulties in extracting charges or energy from such composite systems. Specifically, perovskite NCs are envisioned to be good energy transfer donors due to their high quantum yields, yet energy transfer studies are limited to homonuclear systems[34,35] and perovskite-dye interactions.[36] Furthermore, investigations on distance-dependent properties are lacking. Such experiments were previously performed in-between II-VI semiconductor NCs[37–44] using electrostatic and layer-by-layer assembly techniques, which however are not easily applicable to perovskite NCs due to their labile surface ligands and to their instability issues mentioned above.[45]

Herein, we construct an artificial antenna, where $CsPbBr_3$ NCs are used as light-harvesting energy transfer donors, while Ag NCs are employed as acceptors and catalysts. This system builds up on our previous work, where we used atomic layer deposition (ALD) of amorphous aluminium oxide (AlO_x) to encapsulate and to stabilize perovskite NC films against water, air and light.[46] Now, we extend this idea to construct a $CsPbBr_3/AlO_x/Ag$ multilayer architecture. The conformal nature of the ALD process and the nanoscale control over the separating AlO_x layer (2-21nm), enables us to study for the first time the energy transfer and its distance-dependence from excitonic

perovskite NCs to plasmonic AgNCs. We establish a directional funneling of energy from the perovskite towards the silver, and use this pooled energy to drive a proof-of-concept plasmon-mediated chemical reaction of dye desorption, extending the spectral and spatial absorbance of the catalyst.

The scheme of our antenna is reported in Figure 1A. CsPbBr3 NCs (transmission electron microscopy (TEM) image as inset of Figure 1A), from here on referred to as PeNCs, were spin-coated on glass or silicon substrates, which were pretreated with (3-mercaptopropyl)trimethoxysilane before deposition, to improve NC adhesion and to achieve uniform coverage (Figure S1). An amorphous AlOx layer was then deposited on the PeNC films,

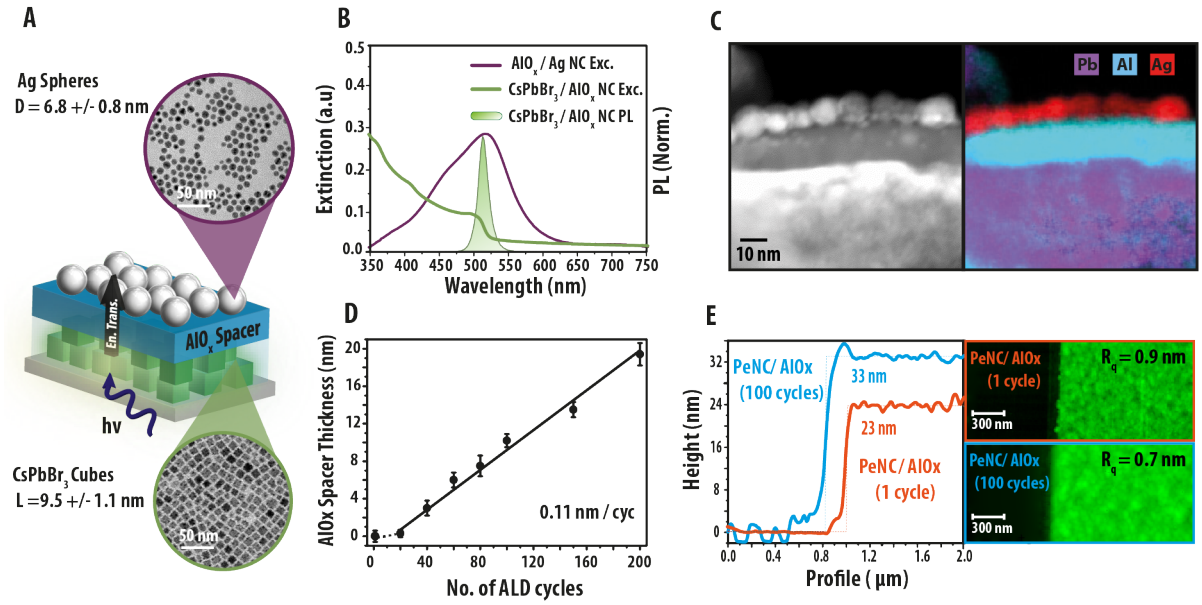

Figure 1: A) Schematic representation of the proposed PeNC/AlO_x/AgNC antenna. Insets show the corresponding TEM images for each NCs. B) Extinction and PL spectra for PeNC/AlO_x and AlO_x/AgNC films, which highlight the spectral overlap. C) Cross-sectional STEM-HAADF image of the PeNC/AlO_x/AgNC antenna and the corresponding EDX map. D) AlO_x spacer thickness for

different numbers of ALD cycles. E) AFM images of the PeNC/AlO_x films after 1 and 100 ALD cycles together with their height profile and root-mean-squared roughness.

following our previously developed ALD method.[46] The thickness of this spacer layer was controlled by varying the number of completed ALD cycles. A minimum of 1 ALD cycle was necessary for all samples to ensure cross-linking of the PeNCs, rendering them insoluble in organic solvents,[47] hence avoiding any washing-off in the subsequent processing steps. To complete the multilayer structure, AgNCs (Figure 1A, TEM inset) were then spincoated on top of the PeNC/AlO_x. This deposition process was properly tuned to obtain a monolayer islands of AgNCs on top of the AlO_x layer (Figure S2) with an Ag NC density of $2.2 \times 10^{15} m^{-2}$ (see Supporting Information). No signs of chemical interaction and/or structural transformations, such as cation-exchange or ion-diffusion,[48–51] were observed between PeNCs and AgNCs (Figure S3).

The overlap between the AgNCs extinction spectrum, from the localized surface plasmon resonance (LSPR), and the PeNCs photoluminescence (PL), shown in Figure 1B, satisfies the energy transfer condition and thus justifies the materials choice. Figure 1C reports a cross-sectional scanning transmission electron microscopy high-angle annular dark-field (STEM-HAADF) image of the final PeNC /AlO_x (15 nm) /AgNC multilayer sample and the corresponding energy-dispersive X-Ray spectroscopy (EDX) map, where all the layers are clearly visible. More images from different parts of the sample can be seen in Figure S4.

To study distance-dependent processes, an accurate estimate of the separation between the donor (PeNCs) and the acceptor (AgNCs) entities is crucial. A systematic investigation of the AlO_x spacer thickness with the number of ALD cycles was performed by atomic force microscopy (AFM) which revealed an AlO_x growth rate of 0.11 nm/cycle (Figures 1D). It must be noted that

below 20 ALD cycles, the growth of an over coating AlO_x layer is very slow, which is consistent with our previous work and with others and attributed to the porous nature of the NC films. [46,52–55] Representative AFM images of PeNC/AlO_x films after 1 and 100 ALD cycles are reported in Figure 1E, along with their area-averaged thickness profiles, while a full set of AFM images can be seen in Figure S5. The minimal change seen in the root-mean-squared surface roughness (R_q) between them points out to the highly conformal deposition of the AlO_x spacer layer. Additionally, it is crucial to indicate the sub-nm root-mean-squared roughness (R_q) observed in all of our films (Figure S6) that justifies the use of ALD deposition for energy transfer measurements.

The PeNC/AlO_x/Ag NC multilayer samples were then used to study the distance-dependent of the energy transfer processes between the excitonic PeNCs and the plasmonic AgNCs by both steady-state and transient spectroscopies. Firstly, the effect of the coupling was investigated by steady-state and transient PL measurements (Figure 2 and S6). The samples were excited at 370-nm where the absorption is dominated by the PeNCs and contributions from Ag NCs are negligible. Subtracted PL decays at the emission peak position of 510-nm in Figure 2A are consistent with shortening of the lifetimes upon the introduction of Ag NCs with decreasing AlO_x spacer thickness. Furthermore, the maximum at around 3ns indicates that quenching primarily occurs at such short timescales. Quenching effects were observed in steady-state measurements, evident by the decrease in the PL quantum yield (QY_{PL}) of PeNCs coupled with Ag NCs (Figure S7). The quenching efficiencies of PeNCs were calculated in two separate ways for comparison; one using PL lifetimes (E_{LT}) and the other using QY_{PL} values (E_{QY}) (see Supporting Information for details, Table S1-S2, Figure S7). It must be noted that for the PeNC/AlO_x (2 nm) sample considerably shorter PL lifetimes and lower QY_{PL} values were recorded compared to the other reference samples with thicker AlO_x spacer layers. This effect was attributed to the surface trap states and incomplete

passivation of the PeNC layer.[46,56] The average distance-dependent quenching, E_{LT} and E_{QY}, as a function of AlO_x spacer layer thickness is reported in Figure 2B and 2C, respectively. It is clear that the PL lifetimes become shorter and the QY is quenched as the distance between the PeNCs and AgNCs decreases. The similar trend between E_{LT} and E_{QY} suggests the primary mechanism of quenching to be through the increase in the non-radiative recombination rate (k_{nr}) rather than the decrease in the radiative recombination rate (k_r), contrary to what has been shown before for dye/metal NC systems.[57] As a matter of fact, the distance-dependent data can be fitted (Figure 2B-C, dashed line) by a non-radiative nanometal surface energy transfer (NSET) formalism, where PeNCs are assumed to be point dipoles transferring energy to an infinite plane of Ag NCs (details in the Supporting Information), giving a characteristic radius of ~6.0 nm for our system. This is in agreement with previously reported radii for quantum dot/metal NC systems.[58]

As NSET was identified to be the main coupling mechanism, one must now consider that the AgNC LSPR can be excited indirectly through the PeNCs due to the spectral overlap seen in Figure 1B. Additional long-range energy exchange phenomena in the weak coupling regime can take place when the LSPR is excited in the vicinity of quantum dots, two of them being the Purcell enhancement and the plasmon-induced resonant energy transfer (PIRET).[59–61] The former, Purcell enhancement, can occur due to the near-field scattering by the plasmonic nanoparticle, that augments the radiative recombination rate of the near-by quantum dot. This in turn increases the quantum dot's QY, which is not what we observe. Furthermore, this effect does not appear in our system even when the LSPR of the AgNCs is excited directly (Figure S8), most likely due to the relatively small size of the AgNCs, where the extinction of the LSPR is dominated by absorption rather than scattering.[62]

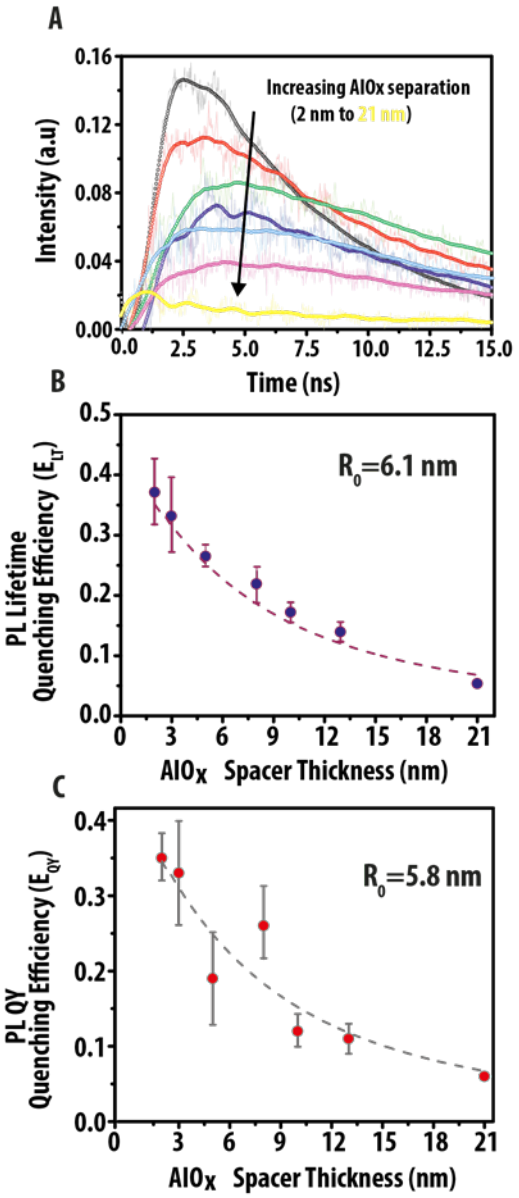

Figure 2: A) Subtracted PL decays of the PeNC at different AlOx thicknesses, obtained from TCSPC measurements at λ_{exc}=370nm by substracting the decay traces of reference PeNC/AlOx from the PeNC/AlOx/AgNC decay traces for each AlOx thickness. B) Quenching efficiency calculated from the PeNC average PL lifetimes over distance C) Quenching efficiency calculated from PeNC QYs over distance. The efficiency values are an average of four set of samples with

error bars representing standard error of the mean. Dashed line in B) and C) represent the NSET fits with their corresponding values for characteristic radii R_0.

The latter energy exchange mechanism, PIRET, is analogous to NSET, where transfer is directed from the plasmonic nanoparticle towards the quantum dot through dipole-dipole coupling. However, no signatures of PIRET was observed in the PL excitation spectra of the PeNC in our system (Figure S8). PIRET is expected to be a coherent isoenergetic process due to the lack of a Stoke's shift, hence the energy is shuffled back and forth from the quantum dots to the plasmonic NCs until one of the dipoles dephases. Hence, the lack of PIRET in our trilayer system can be rationalized by the faster plasmon dephasing times of Ag NC films[63] compared to the slower exciton dephasing times of PeNCs,[64,65] resulting in the final deposition of the energy on the Ag NC side. Overall, the lack of Purcell enhancement and PIRET, combined with the quenching of the PL intensities and shorter lifetimes evidence the unidirectional energy transfer from the PeNC towards the Ag NC through a non-radiative energy transfer process.

Finally, understanding if the energy funneled from the PeNCs to the AgNCs can be used to drive chemical reactions is interesting, considering that no study of this kind has been reported before for PeNCs. In the past decade, numerous reports have shown LSPR-mediated photochemical reactions on metallic NC surfaces.[66–68] While the exact contribution of thermal and charge excitation processes towards these LSPR-mediated reactions is still under debate, there is a common agreement regarding the viability of the approach. One of model the reactions that has been considered for mechanistic studies is the degradation/desorption of the methylene blue (MB) dye from AgNC surfaces.[69,70] Hence, we take this to study the photocatalytic capacity of our PeNC/AlOx/AgNC antenna.

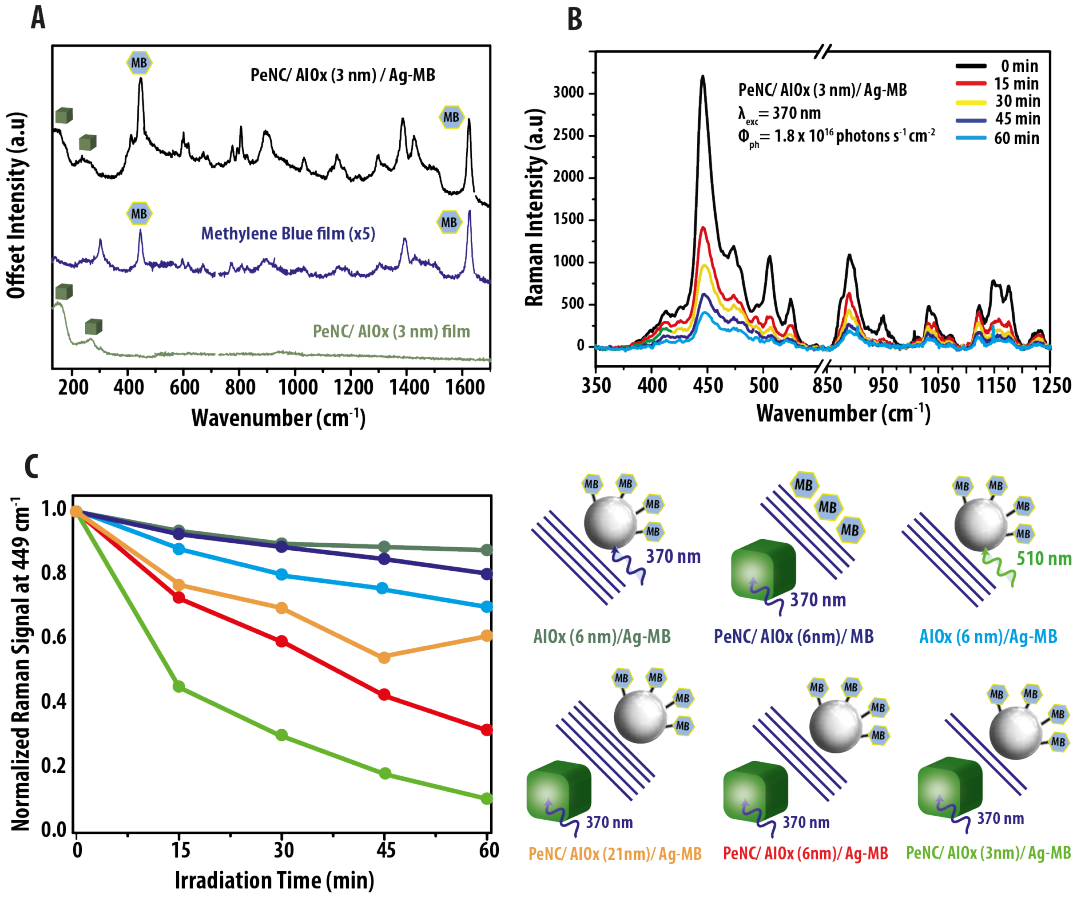

Figure 3: A) Raman spectra of the denoted samples. B) A representative photochemical reaction experiment showing the decrease of the Raman signal for the PeNC/AlOx (3nm)/Ag-MB sample under illumination. C) Normalized Raman signal at 449 cm^{-1} for a number of experiments, as denoted by color coding. All Raman spectra (with the exception of PeNC/AlOx(6nm)/MB, see SI) were gathered by a 633-nm laser and a photon flux of 6.0 x 10^{20} $cm^{-2}s^{-1}$. SERS spectra corresponding to each of these six experiments are reported in Figure S11.

Figure 3A shows the Raman spectra of the PeNC/AlO_x(3 nm)/AgNC-MB structure along with the reference samples. Other than the two peaks at 150 cm^{-1} and 270 cm^{-1}, which were assigned to the

PeNC/AlO_x film, the rest of the spectral features were attributed to the MB molecule, consistent with previous literature.[69–71] A comparison between MB spectra with and without AgNCs clearly demonstrate the surface enhancement effect on the Raman signals and thus evidence the proximity of the dye molecules to the Ag surface. Figure 3B reports the changes in the spectrum of the PeNC/AlO_x(3 nm)/AgNC-MB during illumination. The absence of new and/or shifted peaks at the high wavenumber range excludes the possibility of a reduction or degradation reaction.[71] On the other hand, a decreased intensity of the Raman signal is observed over time.

Sintering of the the Ag NCs under constant illumination was excluded by TEM and UV-vis absorption experiments (Figure S10). Therefore, the decreased signal intensity cannot be attributed to disappearance of the surface enhancement from the reduced Ag surface. One of the viable mechanisms in plasmonic photocatalysis is the chemical interface damping (CID). CID occurs in metal NC-adsorbate systems; hot electrons are generated within a metal NC through LSPR excitation, transiently populating and depositing vibrational energy to the empty adsorbate states, consecutively relaxing back to the metal NC. The excess vibrational energy on the adsorbate can then be utilized for dissociation or desorption.[72] In accordance with this mechanism and with a previous study on MB on Ag surfaces, the decrease of the Raman signals points out to the desorption of the MB dye from the Ag NC surface induced by the plasmon excitation through energy transfer from the PeNCs.

The hypothesis that PeNC to AgNC energy transfer being the driving force behind this MB desorption process was tested by a number of control experiments. Figure 3C shows the normalized signal intensities for the stronger MB signal at 449 cm^{-1}, over illumination time for each set of experiments. Minimal deterioration of the MB signal was observed when AlO_x/Ag-MB was illuminated at 370-nm without the underlying PeNC layer. At this wavelength, there is

negligible LSPR excitation, therefore the slight decrease the intensity is ascribed to heating effects from long term light exposures. Similarly, no significant signal loss was detected when the MB molecules were directly spincoated on the PeNC/AlO_x (6nm) film, without Ag NCs. This rules out the possibility of direct charge or energy transfer processes from the PeNC to the MB molecules. To further test the distance dependence of the MB desorption, the multilayer structures were illuminated at different AlO_x spacer layer thicknesses. While at larger PeNC-AgNC separations MB desorption slows down, it speeds up at smaller separations, in agreement with the PL data shown in Figure 2. It is interesting to note that AlO_x/Ag-MB samples illuminated at the 510-nm LSPR peak with the similar photon flux were less active than all the PeNC/AlO_x/Ag-MB samples. While further investigation is needed, these findings suggest the possibility of increased lifetime of the hot electrons or of the excitation rate as a result of coupling with the excitonic PeNCs.

In conclusion, we propose a novel antenna assembly, enabled by the conformal deposition of AlO_x, to study energy transfer processes for acceptor-donor systems where layer-by-layer assembly methods are not applicable. We use this platform to investigate for the first time distance-dependent interactions of PeNCs donors with nearby acceptor entities, exemplified by plasmonic AgNCs. We couple transient and steady-state PL and absorption spectroscopies to establish unidirectional non-radiative energy transfer from the PeNCs towards the AgNCs. Finally, we demonstrate the photocatalytic capacity of this multilayer system by studying a simple plasmon-mediated reaction (i.e. MB desorption from the AgNC surface). Interestingly, we show that the spectral absorbance of the AgNC can be extended to higher energies with the PeNC antenna and utilized to drive photochemical reactions more efficiently. From a more general perspective, we foresee two main advantages of this multilayer platform. Firstly, on the PeNC side, we show that energy can be extracted from them even if they are buried under a 10-nm overcoating layer. This

opens up the way to both stabilize and utilize them as light-absorbers to catalyze various liquid-phase reactions. Secondly, on the plasmonic photocatalysis side, coupling the metal nanoparticle at a certain energy with a semiconductor light-absorber can improve photocatalytic efficiencies, though the mechanism behind such behavior remains to be investigated.

AUTHOR INFORMATION

Corresponding Author

* Email: raffaella.buonsanti@epfl.ch

Author Contributions

The manuscript was written through contributions of all authors. All authors have given approval to the final version of the manuscript.

ACKNOWLEDGMENT

This work was supported by the Swiss National Science Foundation (AP Energy Grant, project number PYAPP2_166897/1). We thank Dr. Daniele Laub & Dr. Collette Valotton for cross section preparation, Valeria Mantella for help with TEM imaging, Valerie Niemann for providing the silver nanocrystals.

REFERENCES

(1) Scholes, G. D.; Fleming, G. R.; Olaya-Castro, A.; Van Grondelle, R. Lessons from Nature about Solar Light Harvesting. *Nature Chemistry*. **2011**, 763–774.

(2) Brédas, J. L.; Sargent, E. H.; Scholes, G. D. Photovoltaic Concepts Inspired by Coherence Effects in Photosynthetic Systems. *Nature Materials*. **2016**, 35–44.

(3) Lian, S.; Kodaimati, M. S.; Weiss, E. A. Photocatalytically Active Superstructures of Quantum Dots and Iron Porphyrins for Reduction of CO2 to CO in Water. *ACS Nano* **2018**, *12* (1), 568–575.

(4) Kodaimati, M. S.; Lian, S.; Schatz, G. C.; Weiss, E. A. Energy Transfer-Enhanced Photocatalytic Reduction of Protons within Quantum Dot Light-Harvesting–Catalyst Assemblies. *Proc. Natl. Acad. Sci.* **2018**, *115* (33), 8290–8295.

(5) Martindale, B. C. M.; Hutton, G. A. M.; Caputo, C. A.; Reisner, E. Solar Hydrogen Production Using Carbon Quantum Dots and a Molecular Nickel Catalyst. *J. Am. Chem. Soc.* **2015**, *137* (18), 6018–6025.

(6) Kuehnel, M. F.; Creissen, C. E.; Sahm, C. D.; Wielend, D.; Schlosser, A.; Orchard, K. L.; Reisner, E. ZnSe Nanorods as Visible-Light Absorbers for Photocatalytic and Photoelectrochemical H 2 Evolution in Water. *Angew. Chemie Int. Ed.* **2019**, *58*, 5059–5063.

(7) Simon, T.; Bouchonville, N.; Berr, M. J.; Vaneski, A.; Adrovic, A.; Volbers, D.; Wyrwich, R.; Döblinger, M.; Susha, A. S.; Rogach, A. L.; et al. Redox Shuttle Mechanism Enhances Photocatalytic H2 Generation on Ni-Decorated CdS Nanorods. *Nature Materials*. **2014**, 1–6.

(8) Simon, T.; Carlson, M. T.; Stolarczyk, J. K.; Feldmann, J. Electron Transfer Rate vs Recombination Losses in Photocatalytic H2 Generation on Pt-Decorated CdS Nanorods. *ACS Energy Lett.* **2016**, *1* (6), 1137–1142.

(9) Ben-shahar, Y.; Philbin, J. P.; Scotognella, F.; Ganzer, L.; Cerullo, G.; Rabani, E.; Banin,

U. Charge Carrier Dynamics in Photocatalytic Hybrid Semiconductor–Metal Nanorods: Crossover from Auger Recombination to Charge Transfer. *Nano Lett*. **2018**, *18*, 5211–5216.

(10) Ben-Shahar, Y.; Scotognella, F.; Kriegel, I.; Moretti, L.; Cerullo, G.; Rabani, E.; Banin, U. Optimal Metal Domain Size for Photocatalysis with Hybrid Semiconductor-Metal Nanorods. *Nat. Commun*. **2016**, *7*, 1–7..

(11) Nakibli, Y.; Amirav, L. Selective Growth of Ni Tips on Nanorod Photocatalysts. *Chem. Mater*. **2016**, *28* (13), 4524–4527..

(12) Nakibli, Y.; Mazal, Y.; Dubi, Y.; Wächtler, M.; Amirav, L. Size Matters: Cocatalyst Size Effect on Charge Transfer and Photocatalytic Activity. *Nano Lett*. **2018**, *18* (1), 357–364.

(13) Buhbut, S.; Itzhakov, S.; Tauber, E.; Shalom, M.; Hod, I.; Geiger, T.; Garini, Y.; Oron, D.; Zaban, A. Built-in Quantum Dot Antennas in Dye-Sensitized Solar Cells. *ACS Nano* **2010**, *4* (3), 1293–1298.

(14) Timor, R.; Weitman, H.; Waiskopf, N.; Banin, U.; Ehrenberg, B. PEG-Phospholipids Coated Quantum Rods as Amplifiers of the Photosensitization Process by FRET. *ACS Appl. Mater. Interfaces* **2015**, *7* (38), 21107–21114.

(15) Stolarczyk, J. K.; Bhattacharyya, S.; Polavarapu, L. Challenges and Prospects in Solar Water Splitting and CO 2 Reduction with Inorganic and Hybrid Nanostructures. *ACS Catal*. **2018**, *8*, 3602–3635.

(16) Buhbut, S.; Itzhakov, S.; Oron, D.; Zaban, A. Quantum Dot Antennas for Photoelectrochemical Solar Cells. *J. Phys. Chem. Lett*. **2011**, *2* (15), 1917–1924.

(17) Protesescu, L.; Yakunin, S.; Bodnarchuk, M. I.; Krieg, F.; Caputo, R.; Hendon, C. H.; Yang, R. X.; Walsh, A.; Kovalenko, M. V. Nanocrystals of Cesium Lead Halide Perovskites ($CsPbX_3$, X = Cl, Br, and I): Novel Optoelectronic Materials Showing Bright Emission with Wide Color Gamut. *Nano Lett*. **2015**, *15* (6), 3692–3696.

(18) Kang, J.; Wang, L. W. High Defect Tolerance in Lead Halide Perovskite CsPbBr3. *J. Phys. Chem. Lett*. **2017**, *8* (2), 489–493.

(19) Akkerman, Q. A.; Rainò, G.; Kovalenko, M. V; Manna, L. Genesis, Challenges and Opportunities for Colloidal Lead Halide Perovskite Nanocrystals. *Nat. Mater.* **2018**, *17* (5), 394–405.

(20) Yakunin, S.; Protesescu, L.; Krieg, F.; Bodnarchuk, M. I.; Nedelcu, G.; Humer, M.; De Luca, G.; Fiebig, M.; Heiss, W.; Kovalenko, M. V. Low-Threshold Amplified Spontaneous Emission and Lasing from Colloidal Nanocrystals of Caesium Lead Halide Perovskites. *Nat. Commun.* **2015**, *6*, 8056.

(21) Sutherland, B. R.; Sargent, E. H. Perovskite Photonic Sources. *Nat. Photonics* **2016**, *10* (5), 295–302.

(22) Veldhuis, S. A.; Boix, P. P.; Yantara, N.; Li, M.; Sum, T. C.; Mathews, N.; Mhaisalkar, S. G. Perovskite Materials for Light-Emitting Diodes and Lasers. *Adv. Mater.* **2016**, *28* (32), 6804–6834.

(23) Song, J.; Li, J.; Li, X.; Xu, L.; Dong, Y.; Zeng, H. Quantum Dot Light-Emitting Diodes Based on Inorganic Perovskite Cesium Lead Halides (CsPbX3). *Adv. Mater.* **2015**, *27* (44), 7162–7167.

(24) Li, X.; Wu, Y.; Zhang, S.; Cai, B.; Gu, Y.; Song, J.; Zeng, H. $CsPbX_3$ Quantum Dots for Lighting and Displays: Room-Temperature Synthesis, Photoluminescence Superiorities, Underlying Origins and White Light-Emitting Diodes. *Adv. Funct. Mater.* **2016**, *26* (15), 2435–2445.

(25) Xu, Y.; Chen, Q.; Zhang, C.; Wang, R.; Wu, H.; Zhang, X.; Xing, G.; Yu, W. W.; Wang, X.; Zhang, Y.; et al. Two-Photon Pumped Perovskite Semiconductor Nanocrystal Lasers. *J. Am. Chem. Soc.* **2016**, No. 138, 3761–3768.

(26) Zhang, X.; Cao, W.; Wang, W.; Xu, B.; Liu, S.; Dai, H.; Chen, S.; Wang, K.; Sun, X. W. Efficient Light-Emitting Diodes Based on Green Perovskite Nanocrystals with Mixed-Metal Cations. *Nano Energy* **2016**, *30*, 511–516.

(27) Ou, M.; Tu, W.; Yin, S.; Xing, W.; Wu, S.; Wang, H.; Wan, S.; Zhong, Q.; Xu, R. Amino-

Assisted Anchoring of CsPbBr 3 Perovskite Quantum Dots on Porous g-C 3 N 4 for Enhanced Photocatalytic CO 2 Reduction. *Angew. Chemie - Int. Ed.* **2018**, *57* (41), 13570–13574.

(28) Kong, Z. C.; Liao, J. F.; Dong, Y. J.; Xu, Y. F.; Chen, H. Y.; Kuang, D. Bin; Su, C. Y. Core@shell Cspbbr3@zeolitic Imidazolate Framework Nanocomposite for Efficient Photocatalytic Co2 Reduction. *ACS Energy Lett.* **2018**, *3* (11), 2656–2662.

(29) Xu, Y. F.; Yang, M. Z.; Chen, B. X.; Wang, X. D.; Chen, H. Y.; Kuang, D. Bin; Su, C. Y. A CsPbBr3 Perovskite Quantum Dot/Graphene Oxide Composite for Photocatalytic CO2 Reduction. *J. Am. Chem. Soc.* **2017**, *139* (16), 5660–5663.

(30) Wang, H. C.; Lin, S. Y.; Tang, A. C.; Singh, B. P.; Tong, H. C.; Chen, C. Y.; Lee, Y. C.; Tsai, T. L.; Liu, R. S. Mesoporous Silica Particle Integrated with All-Inorganic CsPbBr3 Perovskite Quantum-Dot Nanocomposite (MP-PQDs) with High Stability and Wide Color Gamut Used for Backlight Display. *Angew. Chemie - Int. Ed.* **2016**, 7924–7929.

(31) Yuan, S.; Chen, D.; Li, X.; Zhong, J.; Xu, X. In Situ Crystallization Synthesis of CsPbBr 3 Perovskite Quantum Dot- Embedded Glasses with Improved Stability for Solid-State Lighting and Random Upconverted Lasing. *ACS Appl. Mater. Interfaces* **2018**, *10*, 18918–18926.

(32) Raja, S. N.; Bekenstein, Y.; Koc, M. A.; Fischer, S.; Zhang, D.; Lin, L.; Ritchie, R. O.; Yang, P.; Alivisatos, A. P. Encapsulation of Perovskite Nanocrystals into Macroscale Polymer Matrices: Enhanced Stability and Polarization. *ACS Appl. Mater. Interfaces* **2016**, *8* (51), 35523–35533.

(33) Wei, Y.; Cheng, Z.; Lin, J. An Overview on Enhancing the Stability of Lead Halide Perovskite Quantum Dots and Their Applications in Phosphor-Converted LEDs. *Chemical Society Reviews*. **2019**, 310–350.

(34) de Weerd, C.; Gomez, L.; Zhang, H.; Buma, W. J.; Nedelcu, G.; Kovalenko, M. V.; Gregorkiewicz, T. Energy Transfer between Inorganic Perovskite Nanocrystals. *J. Phys. Chem. C* **2016**, *120* (24), 13310–13315.

(35) Bouduban, M. E. F.; Burgos-Caminal, A.; Ossola, R.; Teuscher, J.; Moser, J. E. Energy and Charge Transfer Cascade in Methylammonium Lead Bromide Perovskite Nanoparticle Aggregates. *Chem. Sci.* **2017**, *8* (6), 4371–4380.

(36) Hofmann, F. J.; Bodnarchuk, M. I.; Protesescu, L.; Kovalenko, M. V; Lupton, J. M.; Vogelsang, J. Exciton Gating and Triplet Deshelving in Single Dye Molecules Excited by Perovskite Nanocrystal FRET Antennae. *J. Phys. Chem. Lett.* **2019**, *10* (5), 1055–1062.

(37) Lunz, M.; Bradley, A. L.; Chen, W.-Y.; Gun 'ko, Y. K. Förster Resonant Energy Transfer in Quantum Dot Layers. *Superlattices Microstruct.* **2010**, *47*, 98–102.

(38) Lunz, M.; Bradley, A. L.; Gerard, V. A.; Byrne, S. J.; Gun'Ko, Y. K.; Lesnyak, V.; Gaponik, N. Concentration Dependence of Förster Resonant Energy Transfer between Donor and Acceptor Nanocrystal Quantum Dot Layers: Effect of Donor-Donor Interactions. *Phys. Rev. B - Condens. Matter Mater. Phys.* **2011**, *83* (11), 1–10.

(39) Franzl, T.; Koktysh, D. S.; Klar, T. A.; Rogach, A. L.; FeldmannN Gaponik, J.; Feldmann, J.; Gaponik, N. Fast Energy Transfer in Layer-by-Layer Assembled CdTe Nanocrystal Bilayers. *Cit. Appl. Phys. Lett* **2004**, *84*, 2904.

(40) Franzl, T.; Klar, T. a.; Schietinger, S.; Rogach, A. L.; Feldmann, J. Exciton Recycling in Graded Gap Nanocrystal Structures. *Nano Lett.* **2004**, *4* (9), 1599–1603.

(41) Achermann, M.; Petruska, M. A.; Crooker, S. A.; Klimov, V. I. Picosecond Energy Transfer in Quantum Dot Langmuir–Blodgett Nanoassemblies. *J. Phys. Chem. B* **2003**, *107* (50), 13782–13787.

(42) Zheng, K.; Žídek, K.; Abdellah, M.; Zhu, N.; Chábera, P.; Lenngren, N.; Chi, Q.; Pullerits, T. Directed Energy Transfer in Films of CdSe Quantum Dots: Beyond the Point Dipole Approximation. *J. Am. Chem. Soc.* **2014**, *136* (17), 6259–6268.

(43) Kodaimati, M. S.; Wang, C.; Chapman, C.; Schatz, G. C.; Weiss, E. A. Distance-Dependence of Interparticle Energy Transfer in the Near-Infrared within Electrostatic Assemblies of PbS Quantum Dots. *ACS Nano* **2017**, No. 11, 5041–5050.

(44) Wang, C.; Weiss, E. A. Accelerating FRET between Near-Infrared Emitting Quantum Dots Using a Molecular J ‐ Aggregate as an Exciton Bridge. *Nano Lett*. **2017**, *17*, 5666–5671.

(45) De Roo, J.; Ibáñez, M.; Geiregat, P.; Nedelcu, G.; Walravens, W.; Maes, J.; Martins, J. C.; Van Driessche, I.; Kovalenko, M. V.; Hens, Z. Highly Dynamic Ligand Binding and Light Absorption Coefficient of Cesium Lead Bromide Perovskite Nanocrystals. *ACS Nano* **2016**, *10*, 2071–2081.

(46) Loiudice, A.; Saris, S.; Oveisi, E.; Alexander, D. T. L.; Buonsanti, R. CsPbBr 3 QD/AlO x Inorganic Nanocomposites with Exceptional Stability in Water, Light, and Heat. *Angew. Chemie - Int. Ed*. **2017**, *56* (36), 10696–10701.

(47) Li, G.; Rivarola, F. W. R.; Davis, N. J. L. K.; Bai, S.; Jellicoe, T. C.; De La Peña, F.; Hou, S.; Ducati, C.; Gao, F.; Friend, R. H.; et al. Highly Efficient Perovskite Nanocrystal Light-Emitting Diodes Enabled by a Universal Crosslinking Method. *Adv. Mater*. **2016**, *28* (18), 3528–3534.

(48) Lu, M.; Zhang, X.; Bai, X.; Wu, H.; Shen, X.; Zhang, Y.; Zhang, W.; Zheng, W.; Song, H.; Yu, W. W.; et al. Spontaneous Silver Doping and Surface. *ACS Energy Lett*. **2018**, *3*, 1571–1577.

(49) Back, H.; Kim, G.; Kim, J.; Kong, J.; Kim, T. K.; Kang, H.; Kim, H.; Lee, J.; Lee, S.; Lee, K. Achieving Long-Term Stable Perovskite Solar Cells: Via Ion Neutralization. *Energy Environ. Sci*. **2016**, *9* (4), 1258–1263.

(50) Van der Stam, W.; Geuchies, J. J.; Altantzis, T.; Van Den Bos, K. H. W.; Meeldijk, J. D.; Van Aert, S.; Bals, S.; Vanmaekelbergh, D.; De Mello Donega, C. Highly Emissive Divalent-Ion-Doped Colloidal CsPb1-XMxBr3 Perovskite Nanocrystals through Cation Exchange. *J. Am. Chem. Soc*. **2017**, *139* (11), 4087–4097.

(51) Saris, S.; Niemann, V.; Mantella, V.; Loiudice, A.; Buonsanti, R. Understanding the Mechanism of Metal-Induced Degradation in Perovskite Nanocrystals. *Nanoscale*, **2019,** *Advance Article*. https://doi.org/10.1039/c9nr06328e.

(52) Liu, Y.; Tolentino, J.; Gibbs, M.; Ihly, R.; Perkins, C. L.; Liu, Y.; Crawford, N.; Hemminger, J. C.; Law, M. PbSe Quantum Dot Field-Effect Transistors with Air-Stable Electron Mobilities above 7 $Cm^2 V^{-1} s^{-1}$. *Nano Lett*. **2013**, *13* (4).

(53) Liu, Y.; Gibbs, M.; Perkins, C. L.; Tolentino, J.; Zarghami, M. H.; Bustamante, J.; Law, M. Robust, Functional Nanocrystal Solids by Infilling with Atomic Layer Deposition. *Nano Lett*. **2011**, *11* (12), 5349–5355.

(54) Pourret, A.; Guyot-Sionnest, P.; Elam, J. W. Atomic Layer Deposition of ZnO in Quantum Dot Thin Films. *Adv. Mater*. **2009**, *21* (2), 232–235.

(55) Valdesueiro, D.; Prabhu, M. K.; Guerra-Nunez, C.; Sandeep, C. S. S.; Kinge, S.; Siebbeles, L. D. A.; De Smet, L. C. P. M.; Meesters, G. M. H.; Kreutzer, M. T.; Houtepen, A. J.; et al. Deposition Mechanism of Aluminum Oxide on Quantum Dot Films at Atmospheric Pressure and Room Temperature. *J. Phys. Chem. C* **2016**, *120* (8), 4266–4275.

(56) Loiudice, A.; Strach, M.; Saris, S.; Chernyshov, D.; Buonsanti, R. Universal Oxide Shell Growth Enables in Situ Structural Studies of Perovskite Nanocrystals during the Anion Exchange Reaction. *J. Am. Chem. Soc*. **2019**, *141*, 8254–8263.

(57) Dulkeith, E.; Ringler, M.; Klar, T. A.; Feldmann, J.; Javier, A. M.; Parak, W. J. Gold Nanoparticles Quench Fluorescence by Phase Induced Radiative Rate Suppression. *Nano Lett*. **2005**, *5* (4), 585–589.

(58) Zhang, X.; Marocico, C. A.; Lunz, M.; Gerard, V. A.; Gun'Ko, Y. K.; Lesnyak, V.; Gaponik, N.; Susha, A. S.; Rogach, A. L.; Bradley, A. L. Wavelength, Concentration, and Distance Dependence of Nonradiative Energy Transfer to a Plane of Gold Nanoparticles. *ACS Nano* **2012**, *6* (10), 9283–9290.

(59) Akselrod, G. M.; Weidman, M. C.; Li, Y.; Argyropoulos, C.; Tisdale, W. A.; Mikkelsen, M. H. Efficient Nanosecond Photoluminescence from Infrared PbS Quantum Dots Coupled to Plasmonic Nanoantennas. *ACS Photonics* **2016**, *3* (10), 1741–1746.

(60) Li, J.; Cushing, S. K.; Meng, F.; Senty, T. R.; Bristow, A. D.; Wu, N. Plasmon-Induced

Resonance Energy Transfer for Solar Energy Conversion. *Nat Phot*. **2015**, *9* (9), 601–607.

(61) Huang, X.; Li, H.; Zhang, C.; Tan, S.; Chen, Z.; Chen, L.; Lu, Z.; Wang, X.; Xiao, M. Efficient Plasmon-Hot Electron Conversion in Ag–CsPbBr 3 Hybrid Nanocrystals. *Nat. Commun*. **2019**, *10* (1), 1–8.

(62) Hlaing, M.; Gebear-Eigzabher, B.; Roa, A.; Marcano, A.; Radu, D.; Lai, C. Y. Absorption and Scattering Cross-Section Extinction Values of Silver Nanoparticles. *Opt. Mater*. **2016**, *58*, 439–444.

(63) Bosbach, J.; Hendrich, C.; Stietz, F.; Vartanyan, T.; Träger, F. Ultrafast Dephasing of Surface Plasmon Excitation in Silver Nanoparticles: Influence of Particle Size, Shape, and Chemical Surrounding. *Phys. Rev. Lett*. **2002**, *89* (25), 2–5.

(64) Bohn, B. J.; Simon, T.; Gramlich, M.; Richter, A. F.; Polavarapu, L.; Urban, A. S.; Feldmann, J. Dephasing and Quantum Beating of Excitons in Methylammonium Lead Iodide Perovskite Nanoplatelets. *ACS Photonics* **2018**, *5* (2), 648–654.

(65) Rainò, G.; Becker, M. A.; Bodnarchuk, M. I.; Mahrt, R. F.; Kovalenko, M. V; Stöferle, T. Superfluorescence from Lead Halide Perovskite Quantum Dot Superlattices. *Nature*. Springer US 2018, pp 671–675.

(66) Aslam, U.; Rao, V. G.; Chavez, S.; Linic, S. Catalytic Conversion of Solar to Chemical Energy on Plasmonic Metal Nanostructures. *Nature Catalysis*. Springer US 2018, pp 656–665.

(67) Mukherjee, S.; Zhou, L.; Goodman, A. M.; Large, N.; Ayala-Orozco, C.; Zhang, Y.; Nordlander, P.; Halas, N. J. Hot-Electron-Induced Dissociation of H2 on Gold Nanoparticles Supported on SiO2. *J. Am. Chem. Soc*. **2014**, *136* (1), 64–67.

(68) Yu, S.; Wilson, A. J.; Heo, J.; Jain, P. K. Plasmonic Control of Multi-Electron Transfer and C-C Coupling in Visible-Light-Driven CO2 Reduction on Au Nanoparticles. *Nano Lett*. **2018**, *18* (4), 2189–2194.

(69) Boerigter, C.; Campana, R.; Morabito, M.; Linic, S. Evidence and Implications of Direct

Charge Excitation as the Dominant Mechanism in Plasmon-Mediated Photocatalysis. *Nat. Commun.* **2016**, *7*, 1–9.

(70) Boerigter, C.; Aslam, U.; Linic, S. Mechanism of Charge Transfer from Plasmonic Nanostructures to Chemically Attached Materials. *ACS Nano* **2016**, *10* (6), 6108–6115.

(71) Nicolai, S. H. A.; Rubim, J. C. Surface-Enhanced Resonance Raman (SERR) Spectra of Methylene Blue Adsorbed on a Silver Electrode. *Langmuir* **2003**, *19* (10), 4291–4294.

(72) Christopher, P.; Xin, H.; Linic, S. Visible-Light-Enhanced Catalytic Oxidation Reactions on Plasmonic Silver Nanostructures. *Nat. Chem.* **2011**, *3* (6), 467–472.